Electronic Supplementary Material (ESI) for Chemical Science.

Supporting Information

Effects of O, S, and P in transition-metal compounds on adsorption and catalytic ability of sulfur cathodes in lithium-sulfur batteries

Meng Du, [a] Jiakang Shi, [a] Yuxiao Shi, [a] Guangxun Zhang, [a] Yan Yan, [a] Pengbiao Geng, [c] Ziqi Tian, [b] and Huan Pang*[a]

[a] *School of Chemistry and Chemical Engineering, Yangzhou University, Yangzhou, 225009, P. R. China*
[b] *Ningbo Institute of Materials Technology and Engineering, Chinese Academy of Sciences, Ningbo, 315201, P. R. China*
[c] *School of Materials Science and Engineering, Suzhou University of Science and Technology, Suzhou, 215009, P. R. China*

Experimental Section

Materials

All of the reagents used in this experiment were analytical grade and they used without further purifications. All chemicals, nickel nitrate hexahydrate ($Ni(NO_3)_2·6H_2O$), cobalt nitrate hexahydrate ($Co(NO_3)_2·6H_2O$), potassium hexacyanoferrate(III) ($K_3[Fe(CN)_6]$), trisodium citrate dihydrate ($Na_3C_6H_5O_7·2H_2O$), sodium hypophosphite (NaH_2PO_2), and sulfur sublimed, were purchased from Shanghai Sinopharm Chemical Reagent Co. Ltd., China. All aqueous solutions were prepared with high-purity de-ionized water (18 MΩ cm).

Synthesis of FeCoNi-PBA nanocubes

In a typical procedure, 1.5 mmol $Co(NO_3)_2·6H_2O$, 0.5 mmol $Ni(NO_3)_2·6H_2O$, and 2.25 mmol $Na_3C_6H_5O_7·2H_2O$ were dissolved in 50 mL deionized water to produce clear solution A. Then, 1 mmol $K_3[Fe(CN)_6]$ was dissolved in 50 mL deionized water to obtain clear solution B. Afterward, the solution B was directly poured into the solution A under stirring at room temperature. After continuous stirring for 10 minutes, the obtained mixed solution was aged at room temperature for 24 h. The product was collected by centrifugation and washed repeatedly with deionized water and ethanol, respectively. The obtained product was designated FeCoNi-PBA.

Synthesis of FeCoNiO@FeCoNi-PBA

The FeCoNi-PBA were annealed at 230 °C (2 °C min^{-1}) in air for 2 h. The as-obtained products were named FeCoNiO@FeCoNi-PBA.

Synthesis of FeCoNiO-1h, FeCoNiO-2h, and FeCoNiO-3h

The FeCoNi-PBA were annealed at 350 °C (2 °C min^{-1}) in air for 2 h, for obtaining FeCoNiO-2h. At the same temperature and calcination time of 1h and 3h, the as-obtained products were

FeCoNiO-1h and FeCoNiO-3h, respectively.

Synthesis of FeCoNiS@FeCoNi-PBA

The FeCoNi-PBA and sulfur powder with a mass ratio of 1:6 were placed in two separate positions in a tube furnace with sulfur powder at the upstream side. Then, the products were heated up to 300 °C with a heating rate of 2 °C min^{-1} and kept at this temperature for 2 h under a N_2 atmosphere. The final products were denoted as FeCoNiS@FeCoNi-PBA.

Synthesis of FeCoNiS-1h, FeCoNiS-2h, and FeCoNiS-3h

The FeCoNi-PBA and sulfur powder with a mass ratio of 1:10 were placed in two separate positions in a tube furnace with sulfur powder at the upstream side. Then, the products were heated up to 350 °C with a heating rate of 2 °C min^{-1} and kept at this temperature for 2 h under a N_2 atmosphere. The final products were denoted as FeCoNiS-2h. Under the same synthesis steps, when the calcination time is 1h and 3h, the as-obtained products are FeCoNiS-1h and FeCoNiS-3h, respectively.

Synthesis of FeCoNiP@FeCoNi-PBA

The FeCoNi-PBA and NaH_2PO_2 with a mass ratio of 1:5 were placed in two separate positions in a tube furnace with NaH_2PO_2 at the upstream side. Then, the products were heated up to 300 °C with a heating rate of 2 °C min^{-1} and kept at this temperature for 30 min under a N_2 atmosphere. The final products were denoted as FeCoNiP@FeCoNi-PBA.

Synthesis of FeCoNiP-1h, FeCoNiP-2h, and FeCoNiP-3h

The FeCoNi-PBA and NaH_2PO_2 with a mass ratio of 1:10 were placed in two separate positions in a tube furnace with NaH_2PO_2 at the upstream side. Then, the products were heated up to 350 °C with a heating rate of 2 °C min^{-1} and kept at this temperature for 2 h under a N_2 atmosphere. The final products were denoted as FeCoNiP-2h. Under the same synthesis steps,

when the calcination time is 1h and 3h, the as-obtained products are FeCoNiP-1h and FeCoNiP-3h, respectively.

Synthesis of FeCoNi-PBA-S, FeCoNiX-1h-S, FeCoNiX-2h-S, FeCoNiX-3h-S, and FeCoNiX@FeCoNi-PBA-S (X = O, S, P)

In terms of FeCoNiP-2h-S, 70 mg sulfur power was first dissolved into the carbon disulfide (CS_2) solution. Then the as-prepared 30 mg FeCoNiP-2h was dispersed in CS_2 under stirring. After CS_2 is completely evaporated from the mixture, the sample is ground and collected. The final products were denoted as FeCoNiP-2h-S. Moreover, FeCoNiP-1h-S, FeCoNiP-3h-S, FeCoNiO-1h-S, FeCoNiO-2h-S, FeCoNiO-3h-S, FeCoNiS-1h-S, FeCoNiS-2h-S, FeCoNiS-3h-S, FeCoNi-PBA-S, FeCoNiO@FeCoNi-PBA-S, FeCoNiS@FeCoNi-PBA-S, and FeCoNiP@FeCoNi-PBA-S, were also prepared via the same synthetic procedure.

Characterization

The XRD patterns were performed by Rigaku MiniFlex 600 with Cu Kα radiation of 40 KV (λ = 1.5418 Å). SEM images were obtained by Zeiss-Supra 55 microscope at an acceleration voltage of 5 KV. TEM and EDX elemental mapping scans were recorded using Tecnai G2 F30 S-TWIN at an acceleration voltage of 300 KV. The N_2 adsorption-desorption isothermals were obtained by Autosorb-IQ3. Raman spectra were obtained via INVIA REFLEX (Renishaw), in the range 150-4000 cm^{-1}. XPS analysis was carried out using Thermo Scientific ESCALAB 250Xi Xray photoelectron spectrometer with Al Kα radiation as the excitation source. The accurate sulfur mass on each electrode was calculated according to the elemental analysis data from Elementar, VarioELcube Co. (C, H, N, S mode). Fourier transform infrared (FTIR) transmission spectra were obtained on a BRUKER-EQUINOX-55 IR spectrophotometer.

Adsorption and soaking tests

For the adsorption test, 20 mg FeCoNiO-2h, FeCoNiS-2h, and FeCoNiP-2h, were soaked in 3 mL Li_2S_4 solution (10 mmol L^{-1}). The Li_2S_4 solution were prepared in a solvent mixture of 1,3-dioxolane (DOL) and 1,2-dimethoxyethane (DME) (1:1 in volume) according to the reaction equation:

$3S + Li_2S \rightleftarrows Li_2S_4$

UV-vis spectra of the above solutions (diluted 5 times before testing) were recorded by using a UV2550 instrument (Shimadzu, Japan). The concentration variation of polysulfides in these solutions was detected from the UV-vis spectra.

DFT calculation

First-principles calculations were performed using the projector augmented wave (PAW) method,[1] as implemented in the Vienna ab initio simulation package (VASP).[2] Plane wave energy cutoff was set at 420 eV. Electron correlation energy was computed using the Perdew-Burke-Ernzerhof (PBE) type functional (spin polarized) within the generalized gradient approximation (GGA).[3] Grimme's dispersion correction was incorporated to account for the van der Waals interaction.[4] The Brillouin zone was sampled using a Γ-centered Monkhorst-Pack K-point grid with a spacing of 0.04 $Å^{-1}$. Convergence criterions for energy and force were set at 10^{-6} eV and 0.02 eV/Å, respectively.

Electrochemical Measurements

Electrode preparation of FeCoNi-PBA-S, FeCoNiX@FeCoNi-PBA-S, FeCoNiX-1h-S, FeCoNiX-2h-S, and FeCoNiX-3h-S: The slurry was mixed with sample powder, Super P and Polyvinylidene Fluoride (PVDF) in a weight ratio of 7:2:1 in N-methyl-2-pyrrolidone (NMP) as dispersant. Then the slurry was cast on the Al foil (the thickness is 20 nm) and dried overnight at 60 °C under

vacuum. The obtained working electrodes were cut to obtain circular electrodes with a diameter of 12 mm. The accurate sulfur mass on each electrode was calculated according to the elemental analysis data from Elementar, VarioELcube Co. The loading of active sulfur was ~1.2 mg cm^{-2}. The CR 2032-type coin cells were fabricated using the working electrode, lithium foil as the counter and anode electrode, Celgard 2400 as the separator. The electrolyte was used 1.0 M lithium bis(trifluoromethanesulfonyl)imide (LiTFSI Sigma-Aldrich (USA), 99.95%) in DOL (Sigma-Aldrich (USA), 99.0%) and DME (Junsei (Japan), 99.0%) (volume ratio, 1:1). 30 µL of electrolyte was used in the fabrication of each Li-S cell in an argon-filled glove box. The value of electrolyte/sulfur (E/S) ratio is ~22 µL mg^{-1}. The galvanostatic charge/discharge (GCD) tests were estimated in the voltage window of 1.7-2.7 V. The rate capability was also tested by varying the current density from 0.1 C to 1 C (1 C = 1675 mA g^{-1}) on a battery measurement system (CT2001A, Wuhan Land, China) at room temperature. Cyclic voltammetry (CV) and electrochemical impedance spectroscopy (EIS) curves were measured on an electrochemical workstation (CHI660E, Chenhua, Shanghai, China).

In situ UV-vis measurement

The cathode slurry comprised of an active material powder FeCoNiX-2h-S, Super P, and PVDF with a mass ratio of 7:2:1. Then, the nickel foam was selected as the collector (1 × 0.6 cm^2). The sulfur mass loading on the electrode was ~6 mg cm^{-2}, and the current density is 0.05 C. In situ UV-vis cells were assembled using FeCoNiX-2h-S electrode as the cathodes and Li metal as the anode, using a custom made in situ cuvette. In situ cuvette cell was assembled in an Ar filled glove box and sealed in 3 mL of Li-S electrolyte. UV-vis absorption spectra (UV-vis, Shimadzu UVmini-1280 spectrophotometer) were used to detect the concentration and

elemental chemical states of the LiPS.

In situ XRD measurement

In situ XRD was performed on X-ray diffractometer (MiniFlex600-C) and a cell mould with Be. The mass ratio of slurry is the same as in situ UV-vis test, and sulfur area mass loading on the electrode was 1.3 mg cm^{-2}, and the current density is 0.05 C. The current collector is Al foil.

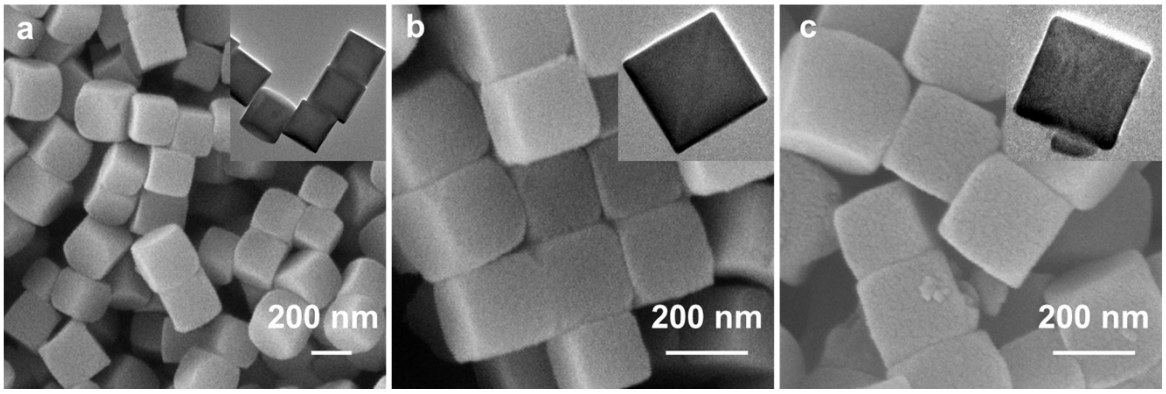

Figure S1. SEM and TEM images of (a, b) FeCoNi-PBA and (c) FeCoNi-PBA-S.

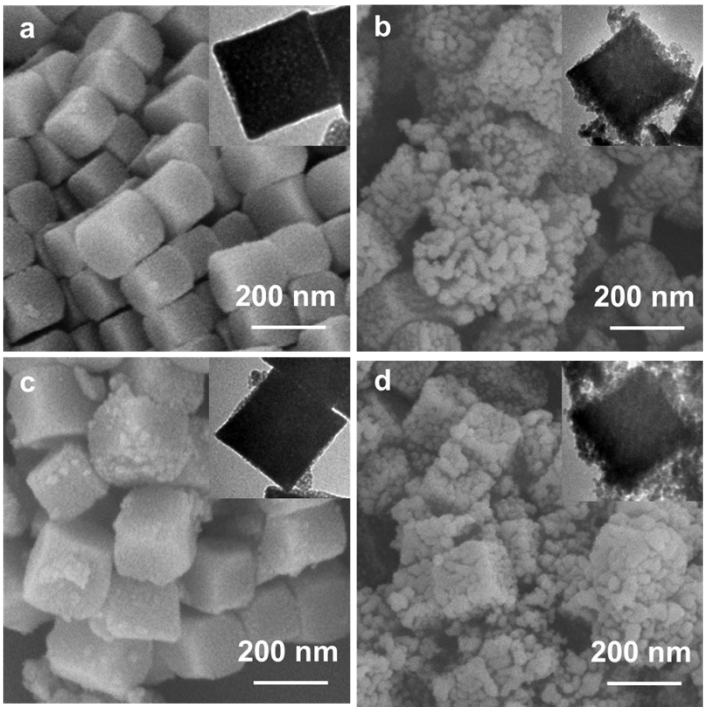

Figure S2. SEM and TEM images of (a) FeCoNiO-1h, (b) FeCoNiO-3h, (c) FeCoNiO-1h-S, and (d) FeCoNiO-3h-S.

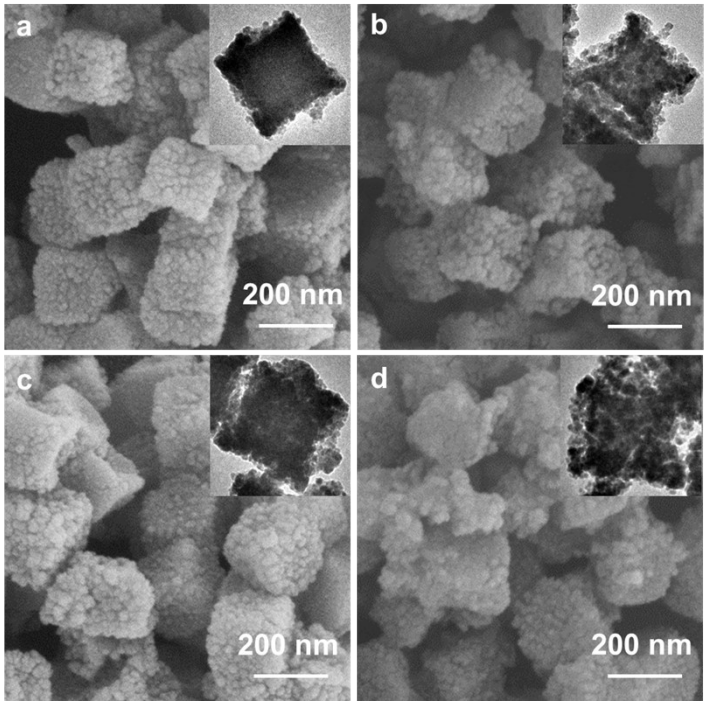

Figure S3. SEM and TEM images of (a) FeCoNiS-1h, (b) FeCoNiS-3h, (c) FeCoNiS-1h-S, and (d) FeCoNiS-3h-S.

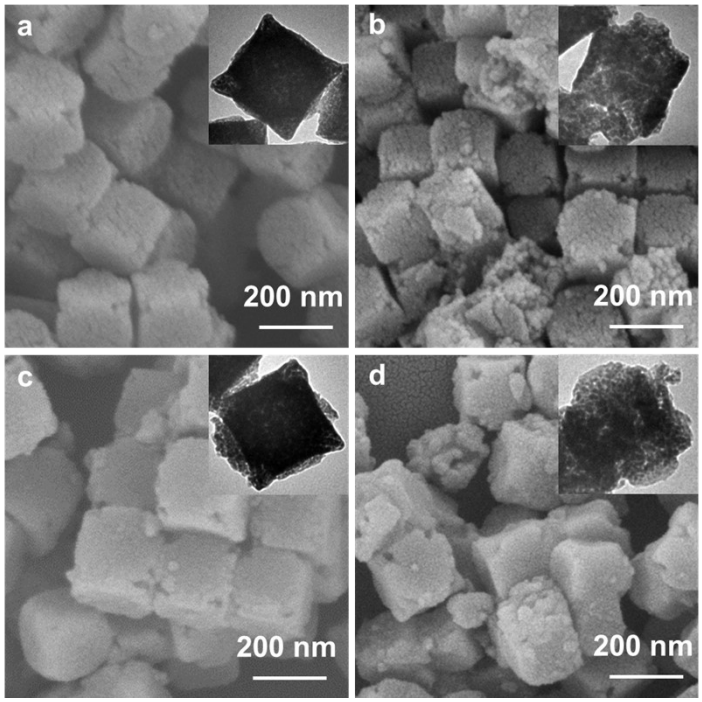

Figure S4. SEM and TEM images of (a) FeCoNiP-1h, (b) FeCoNiP-3h, (c) FeCoNiP-1h-S, and (d) FeCoNiP-3h-S.

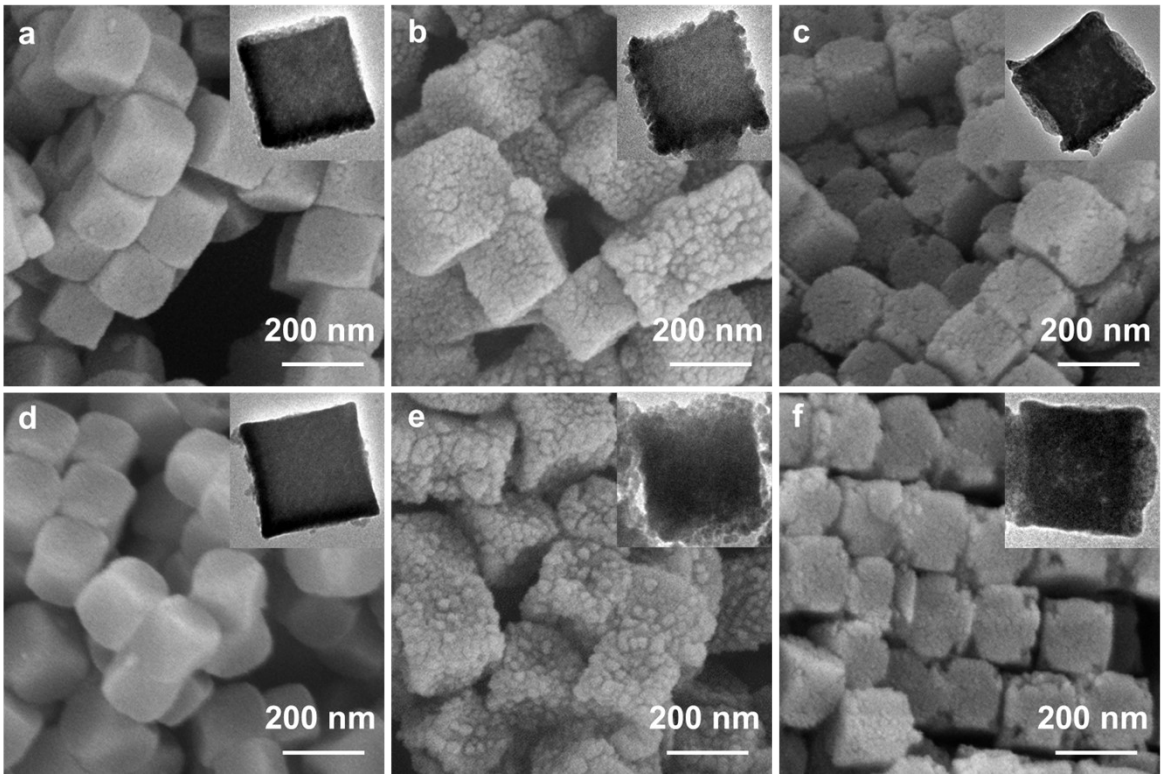

Figure S5. SEM and TEM images of (a) FeCoNiO@FeCoNi-PBA, (b) FeCoNiS@FeCoNi-PBA, (c) FeCoNiP@FeCoNi-PBA, (d) FeCoNiO@FeCoNi-PBA-S, (e) FeCoNiS@FeCoNi-PBA-S, and (f) FeCoNiP@FeCoNi-PBA-S.

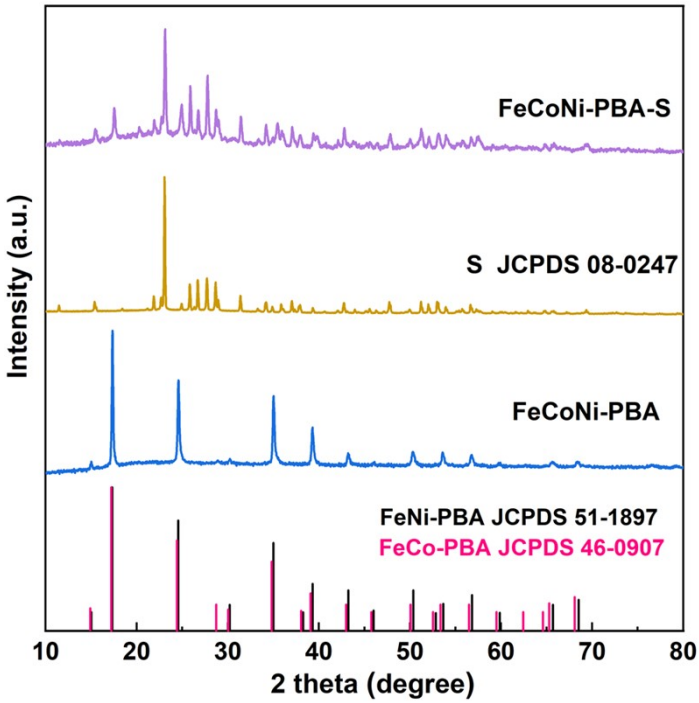

Figure S6. XRD patterns of FeCoNi-PBA and FeCoNi-PBA-S.

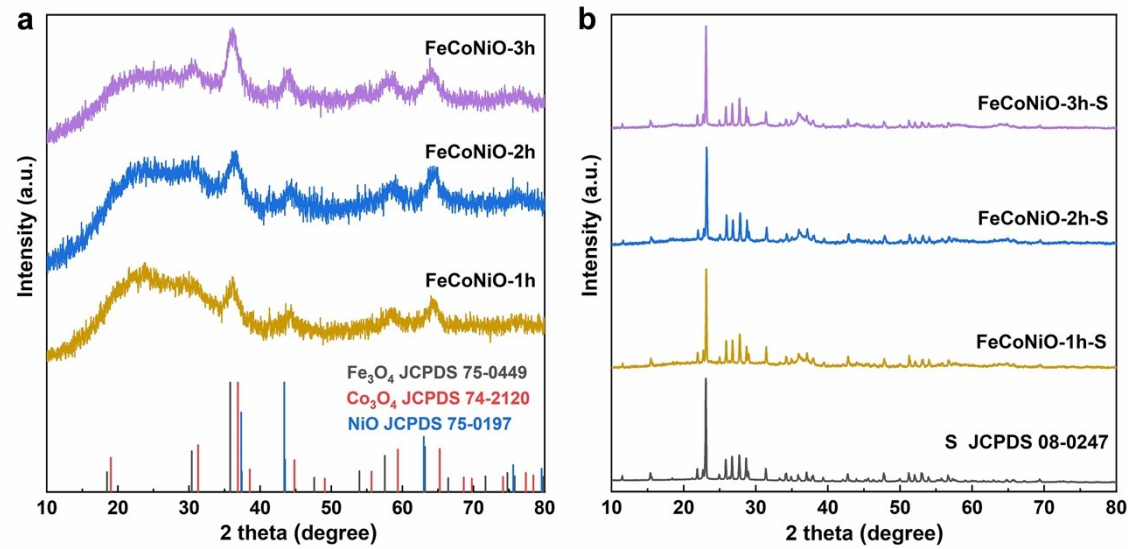

Figure S7. (a) XRD patterns of FeCoNiO-1h, FeCoNiO-2h, and FeCoNiO-3h. (b) XRD patterns of FeCoNiO-1h-S, FeCoNiO-2h-S, and FeCoNiO-3h-S.

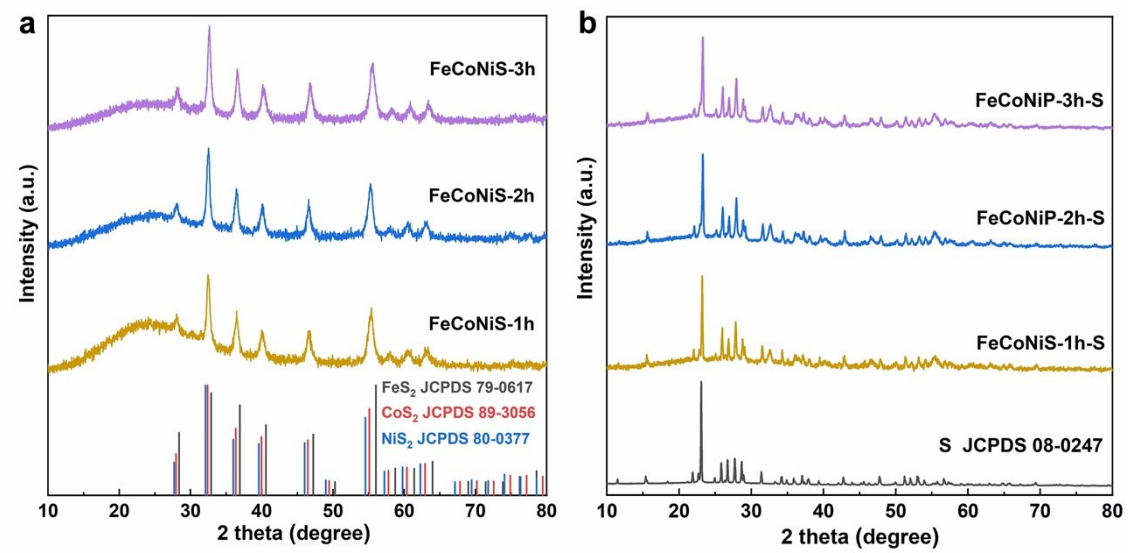

Figure S8. (a) XRD patterns of FeCoNiS-1h, FeCoNiS-2h, and FeCoNiS-3h. (b) XRD patterns of FeCoNiS-1h-S, FeCoNiS-2h-S, and FeCoNiS-3h-S.

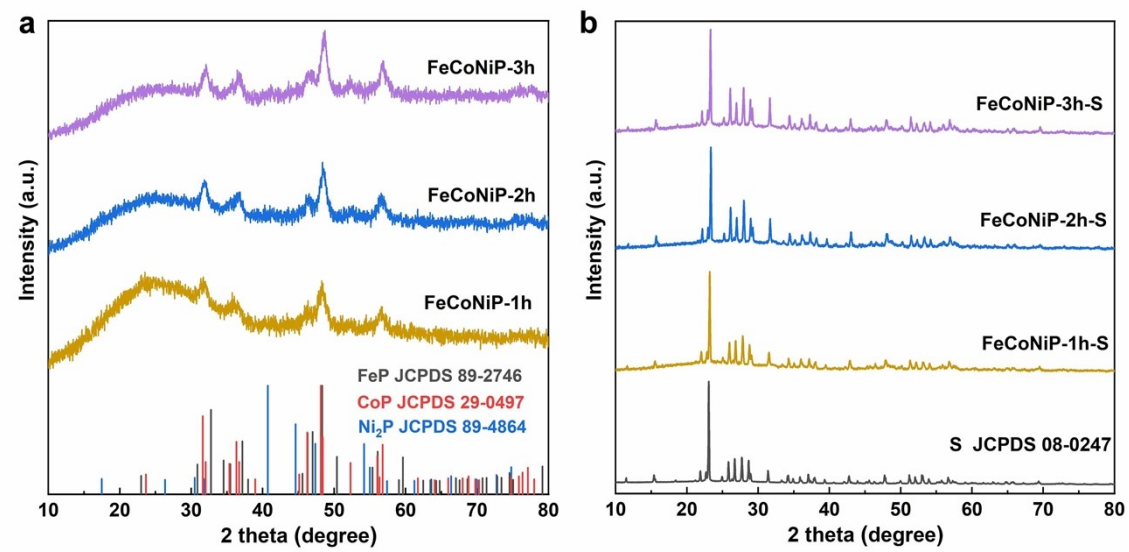

Figure S9. (a) XRD patterns of FeCoNiP-1h, FeCoNiP-2h, and FeCoNiP-3h. (b) XRD patterns of FeCoNiP-1h-S, FeCoNiP-2h-S, and FeCoNiP-3h-S.

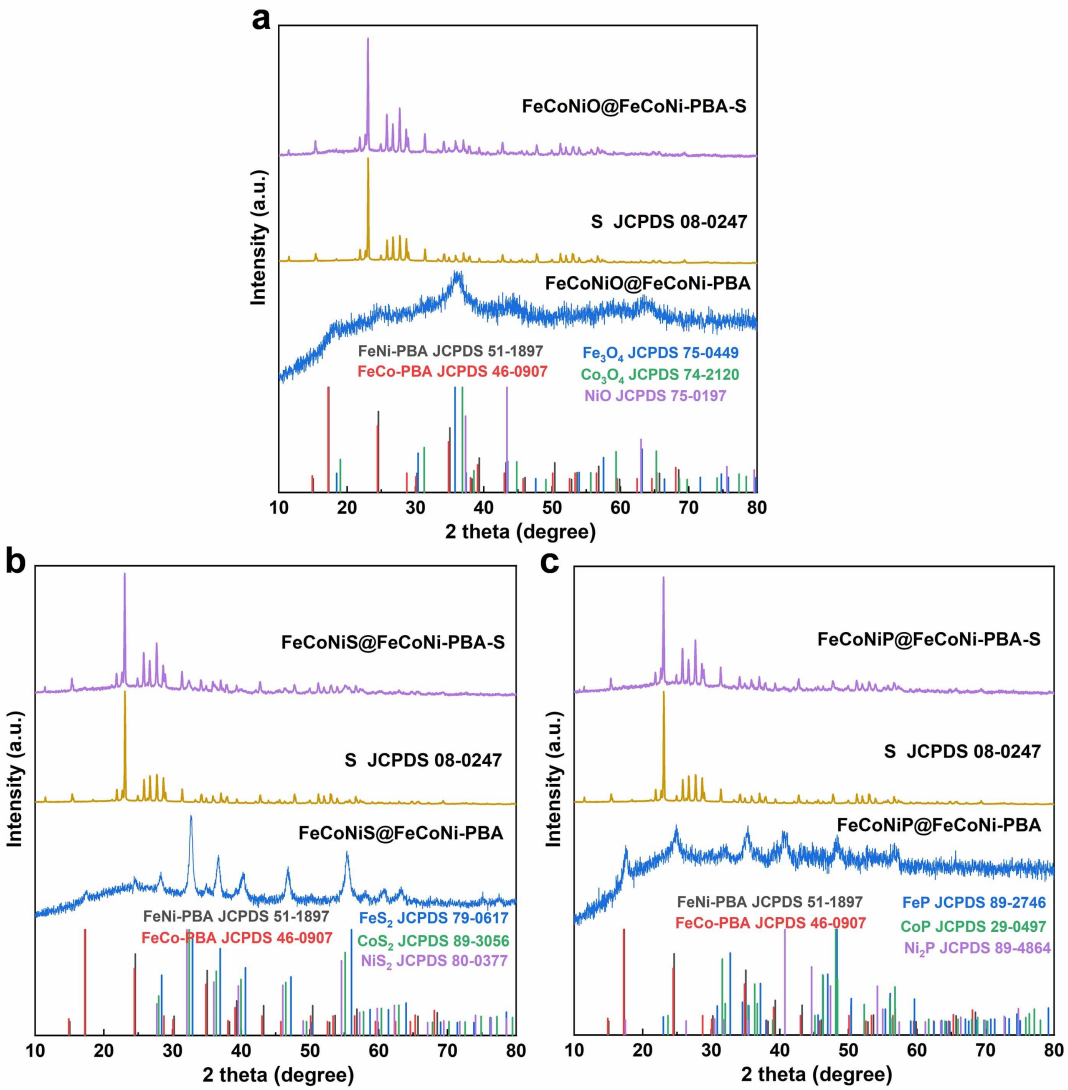

Figure S10. (a) XRD patterns of FeCoNiO@FeCoNi-PBA and FeCoNiO@FeCoNi-PBA-S. (b) XRD patterns of FeCoNiS@FeCoNi-PBA and FeCoNiS@FeCoNi-PBA-S. (c) XRD patterns of FeCoNiP@FeCoNi-PBA and FeCoNiP@FeCoNi-PBA-S.

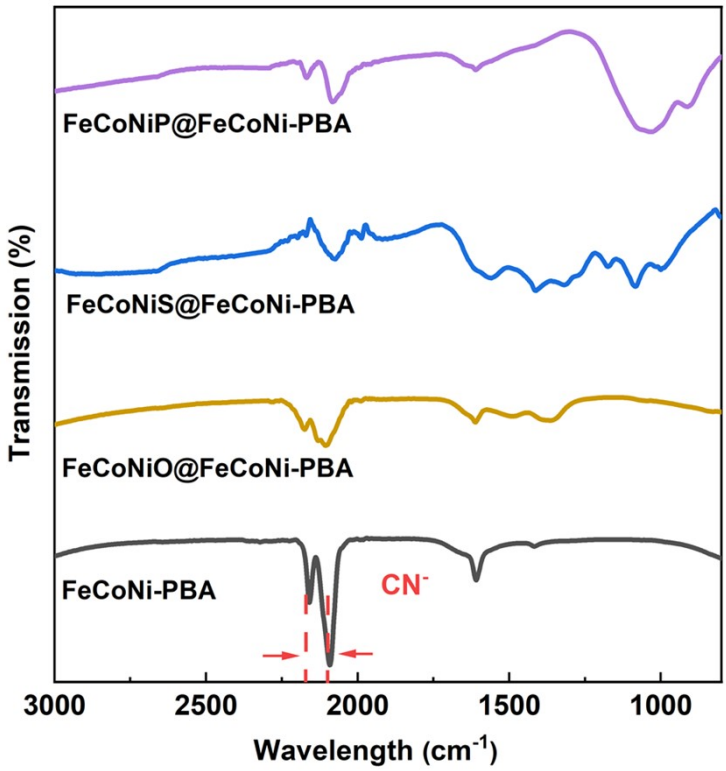

Figure S11. FTIR spectrum of FeCoNi-PBA and FeCoNiX@FeCoNi-PBA.

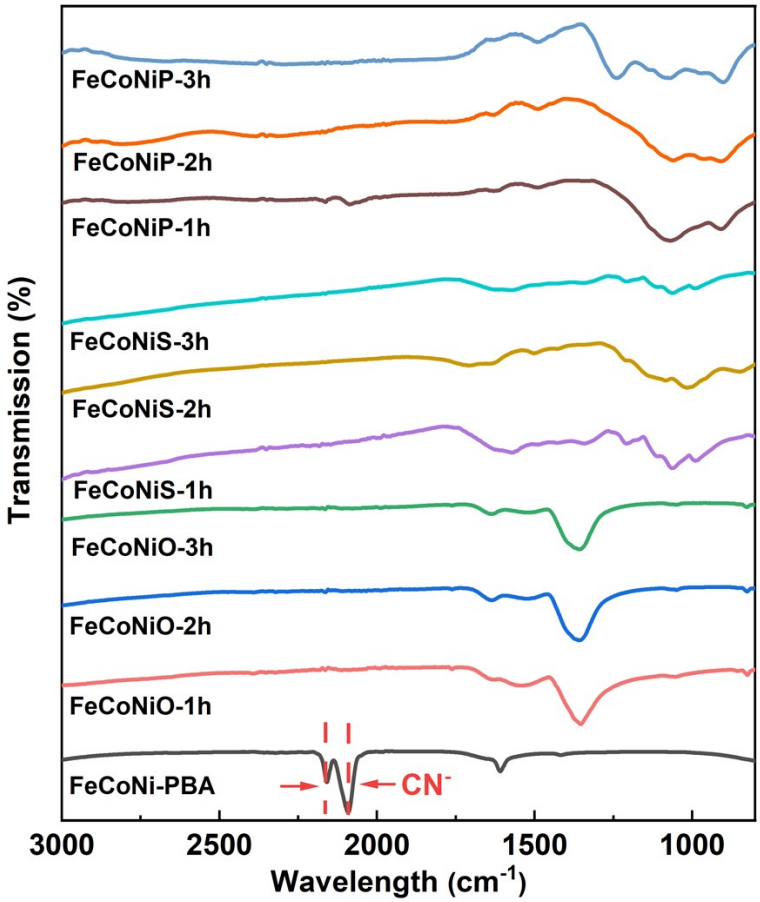

Figure S12. FTIR spectrum of FeCoNi-PBA, FeCoNiX-1h, FeCoNiX-2h, and FeCoNiX-3h.

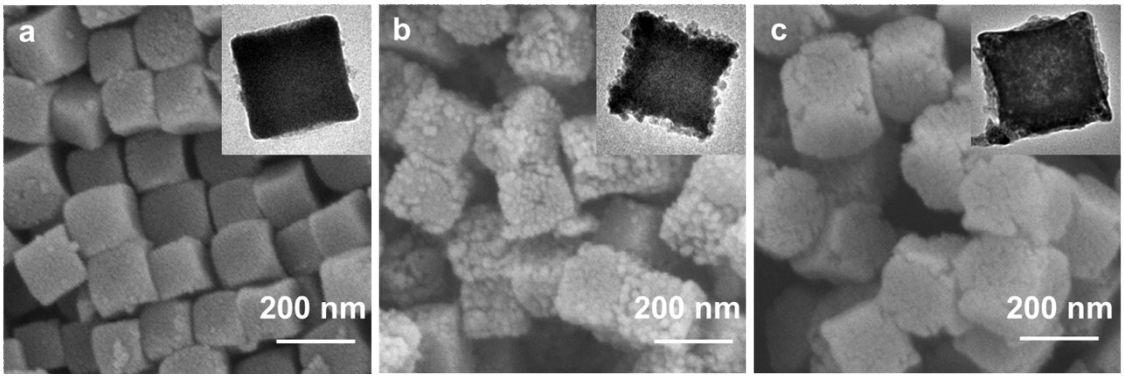

Figure S13. SEM and TEM images of (a) FeCoNiO-2h-S, (b) FeCoNiS-2h-S and (c) FeCoNiP-2h-S.

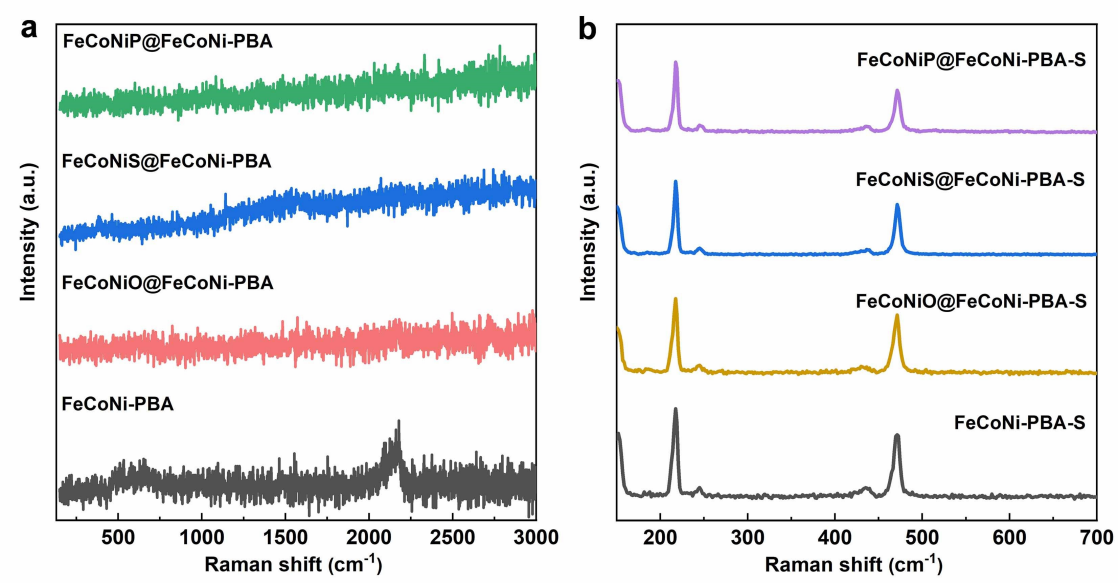

Figure S14. (a) Raman spectra of FeCoNi-PBA and FeCoNiX@FeCoNi-PBA. (b) Raman spectra of FeCoNi-PBA-S and FeCoNiX@FeCoNi-PBA-S.

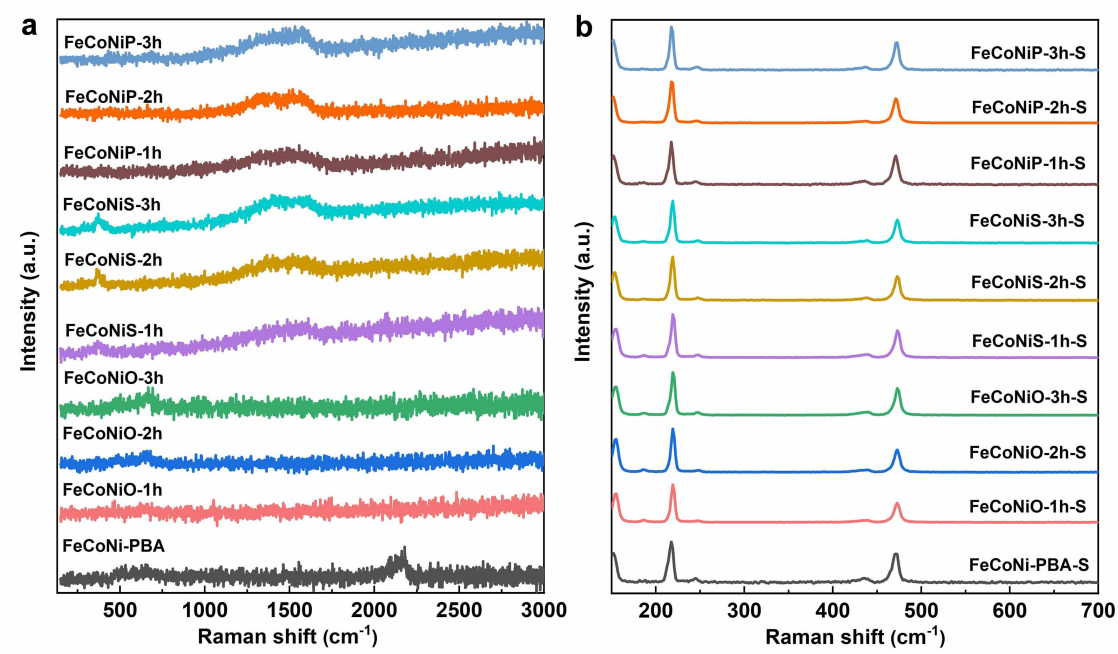

Figure S15. (a) Raman spectra of FeCoNi-PBA, FeCoNiX-1h, FeCoNiX-2h, and FeCoNiX-3h. (b) Raman spectra of FeCoNi-PBA-S, FeCoNiX-1h-S, FeCoNiX-2h-S, and FeCoNiX-3h-S.

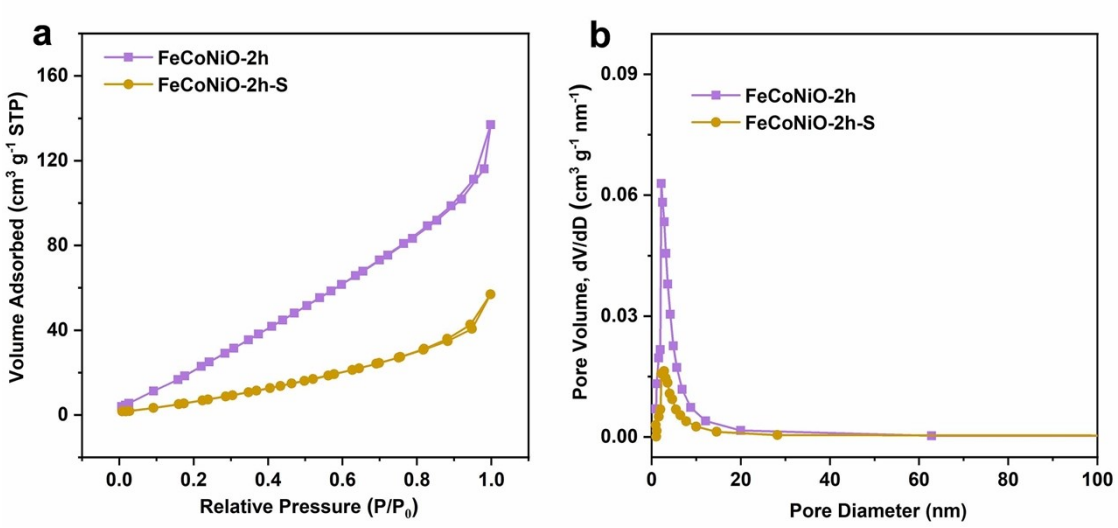

Figure S16. N_2 adsorption-desorption isotherms and pore size distribution of FeCoNiO-2h and FeCoNiO-2h-S.

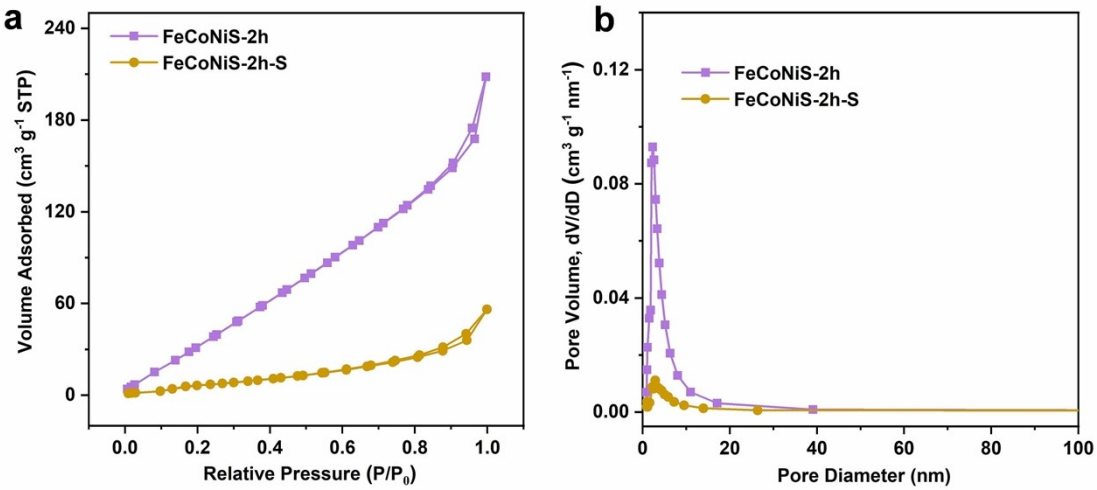

Figure S17. N_2 adsorption-desorption isotherms and pore size distribution of FeCoNiS-2h and FeCoNiS-2h-S.

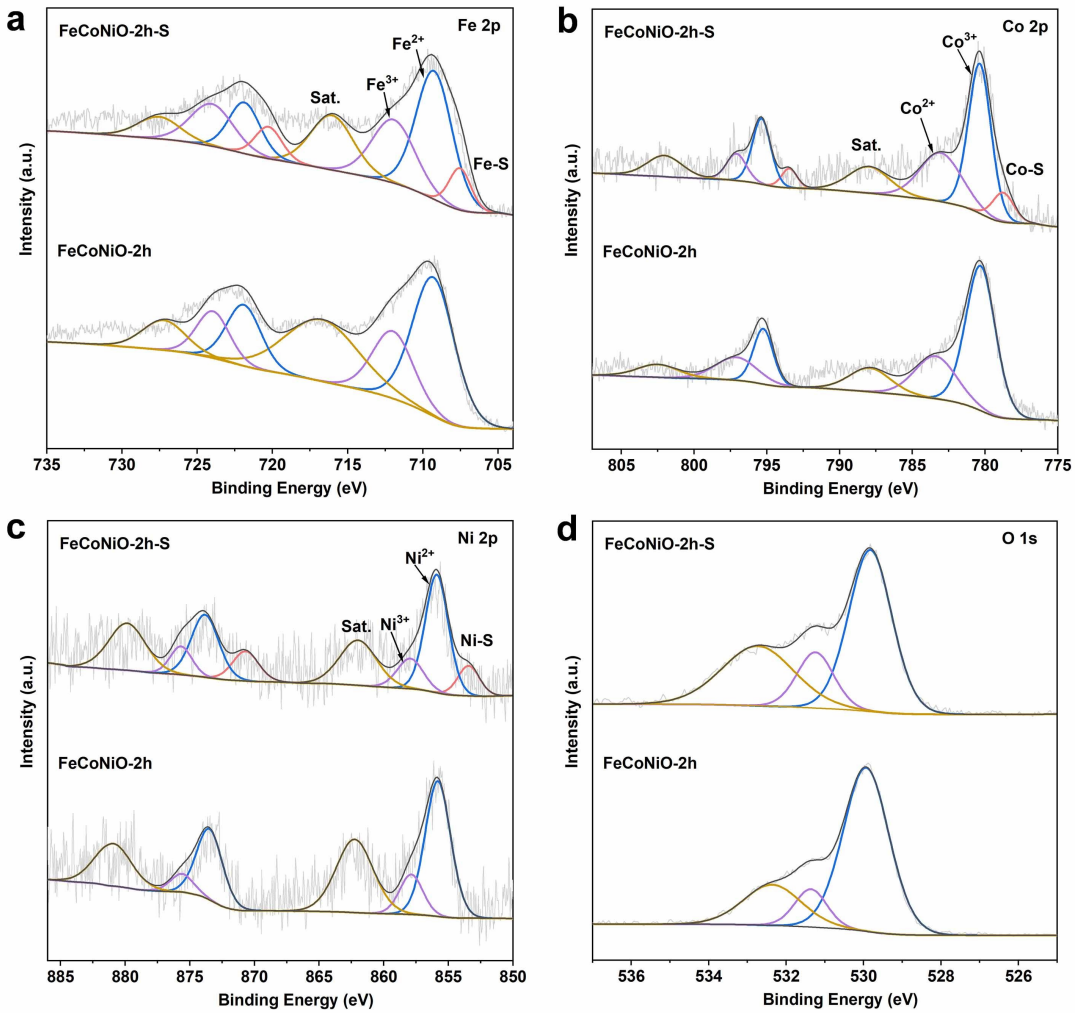

Figure S18. High-resolution XPS spectra of (a) Fe 2p, (b) Co 2p, (c) Ni 2p, (d) O 1s of FeCoNiO-2h and FeCoNiO-2h-S.

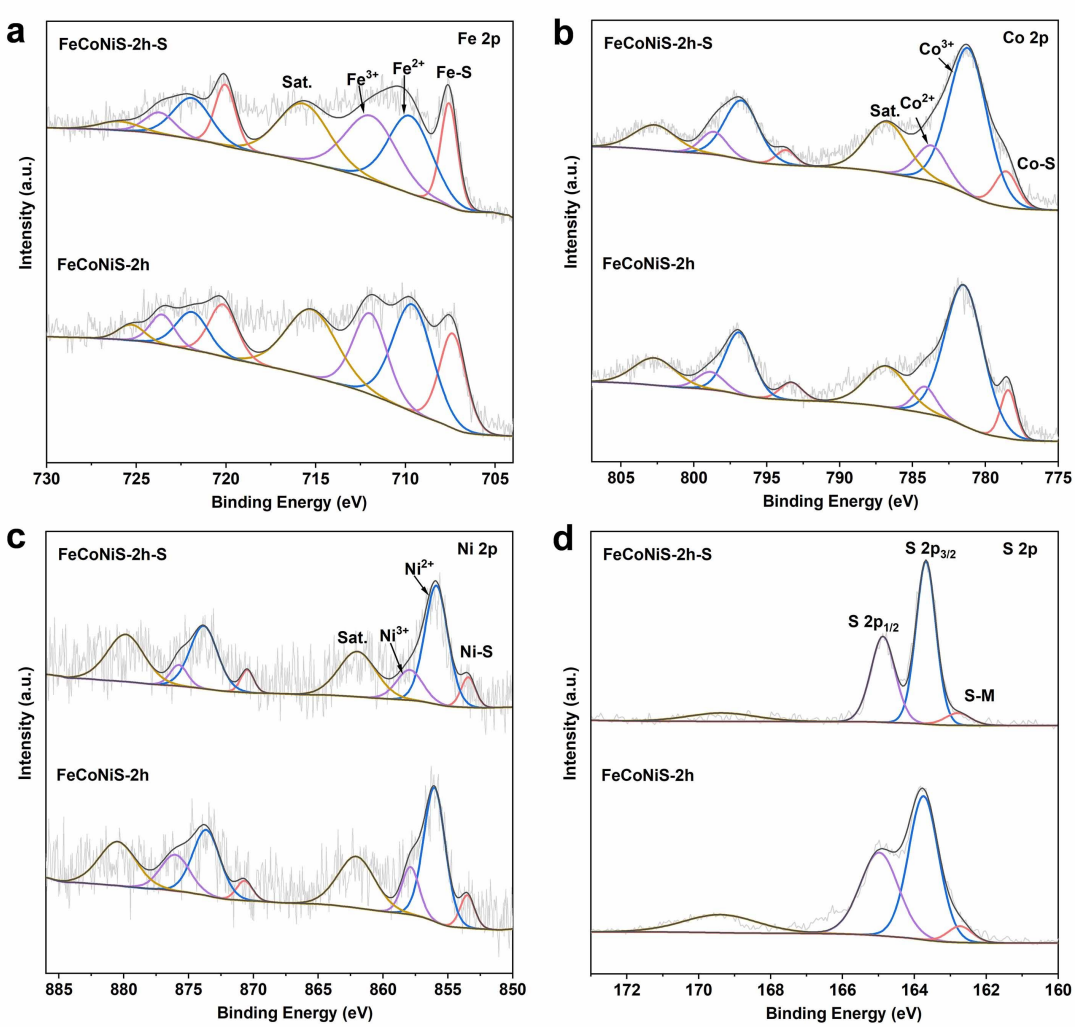

Figure S19. High-resolution XPS spectra of (a) Fe 2p, (b) Co 2p, (c) Ni 2p, (d) S 2p of FeCoNiS-2h and FeCoNiS-2h-S.

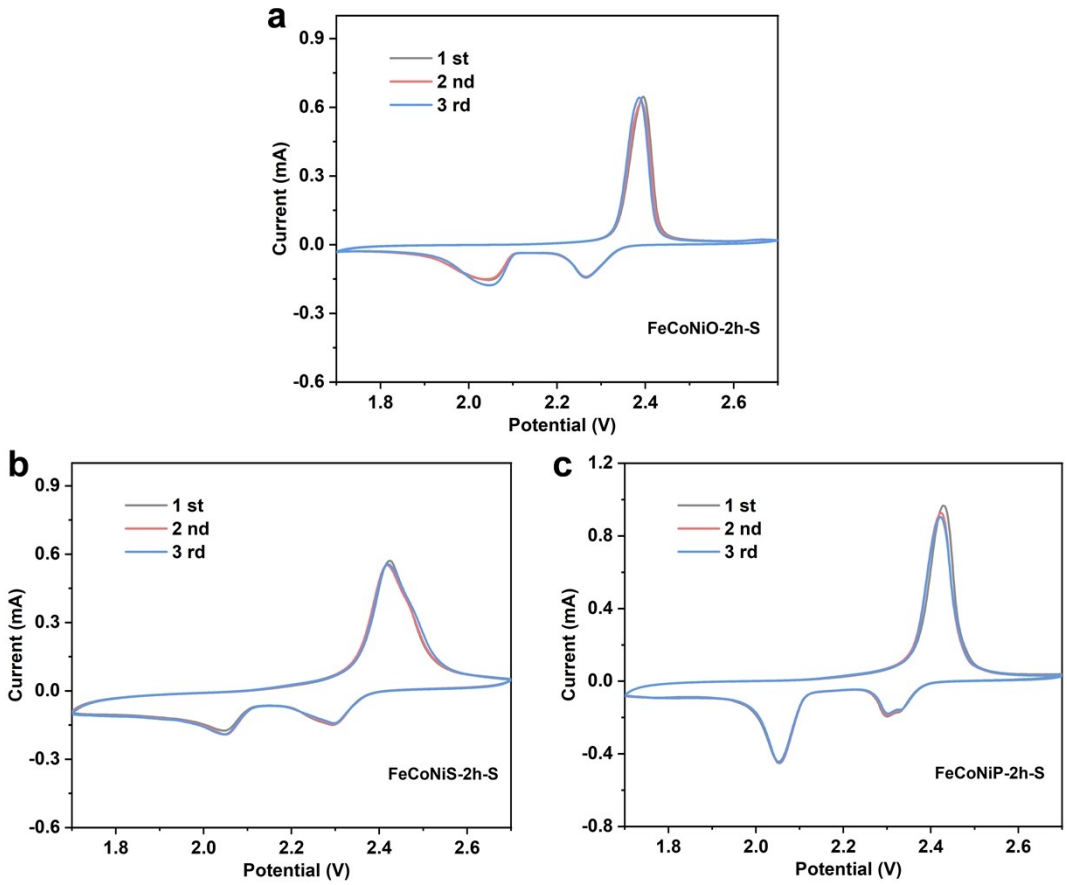

Figure S20. CV curves of the first third cycles of (a) FeCoNiO-2h-S, (b) FeCoNiS-2h-S, and (c) FeCoNiP-2h-S.

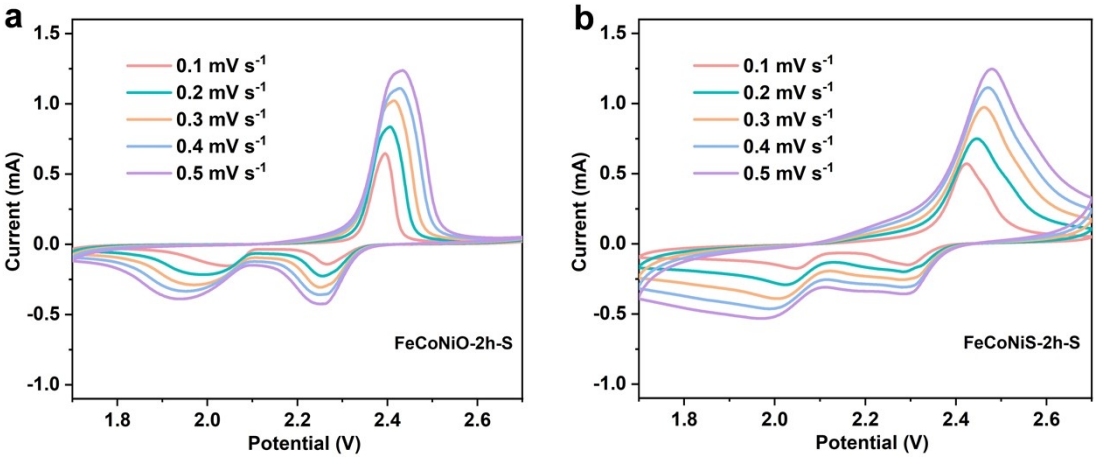

Figure S21. CV curves at different scan rates of (a) FeCoNiO-2h-S and (b) FeCoNiS-2h-S.

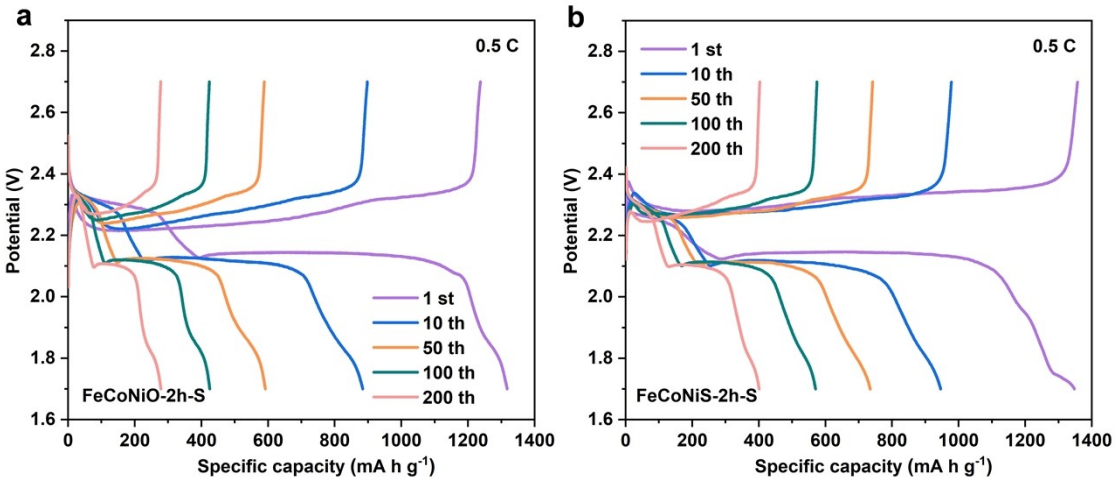

Figure S22. GCD profiles of (a) FeCoNiO-2h-S and (b) FeCoNiS-2h-S at 0.5 C.

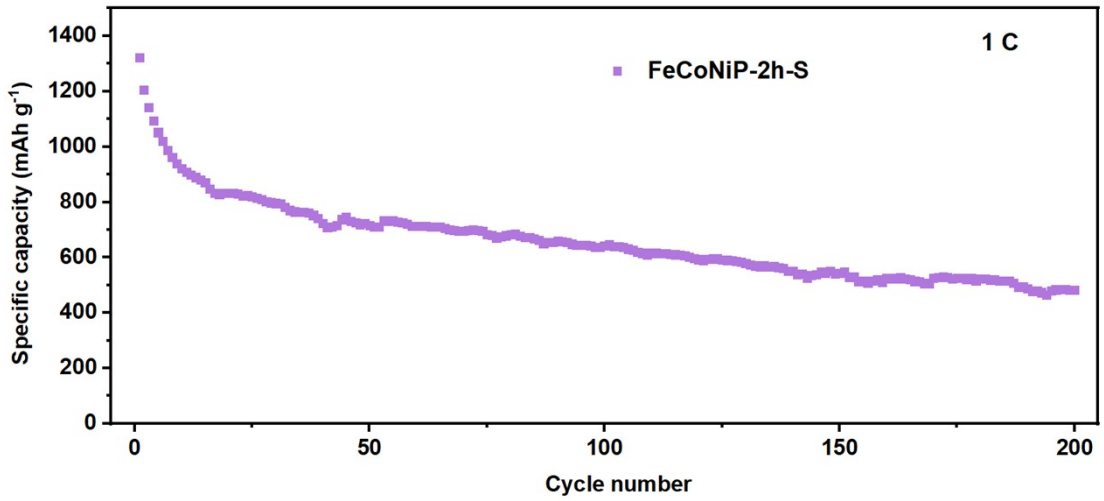

Figure S23. Cycle performance of FeCoNiP-2h-S at 1 C over 200 cycles.

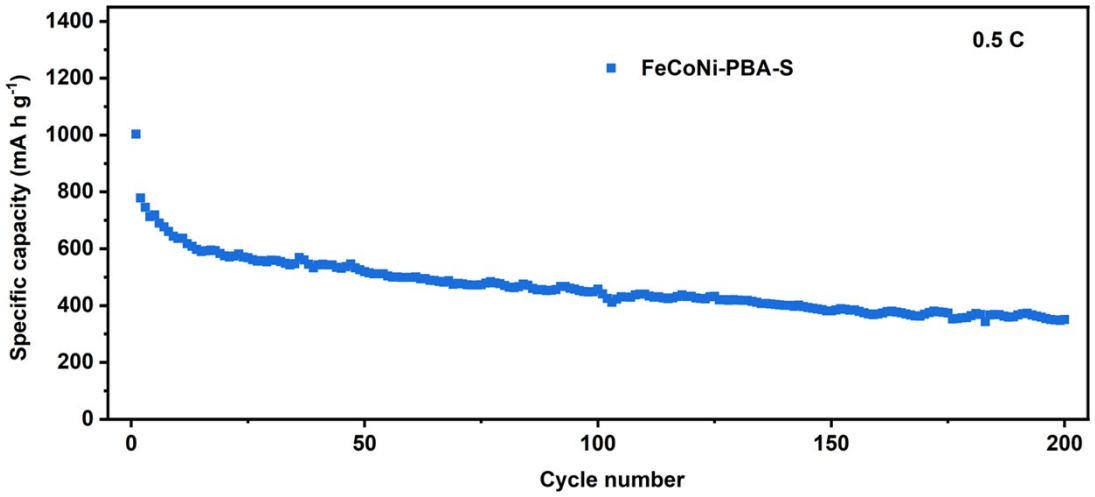

Figure S24. Cycle performance of FeCoNi-PBA-S at 0.5 C over 200 cycles.

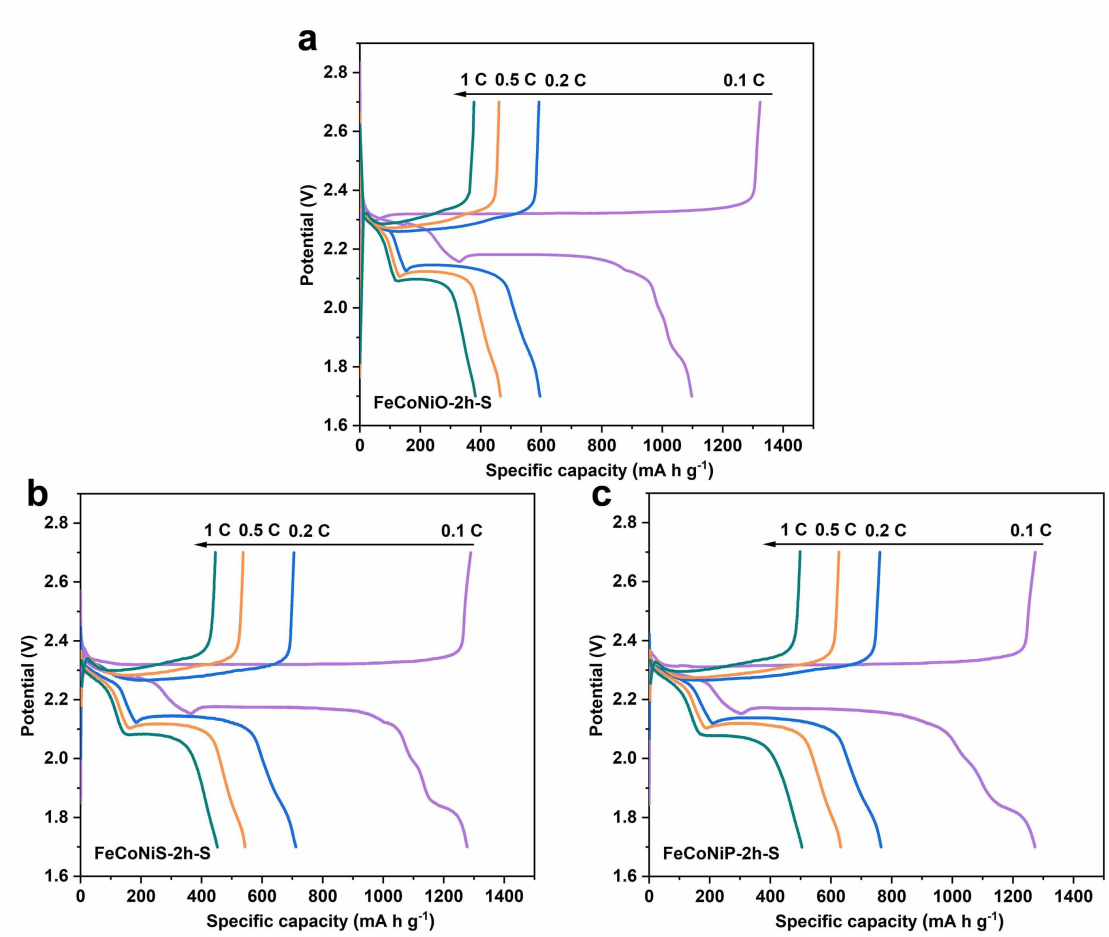

Figure S25. GCD profiles of (a) FeCoNiO-2h-S, (b) FeCoNiS-2h-S, and (c) FeCoNiP-2h-S at 0.1, 0.2, 0.5 and 1.0 C.

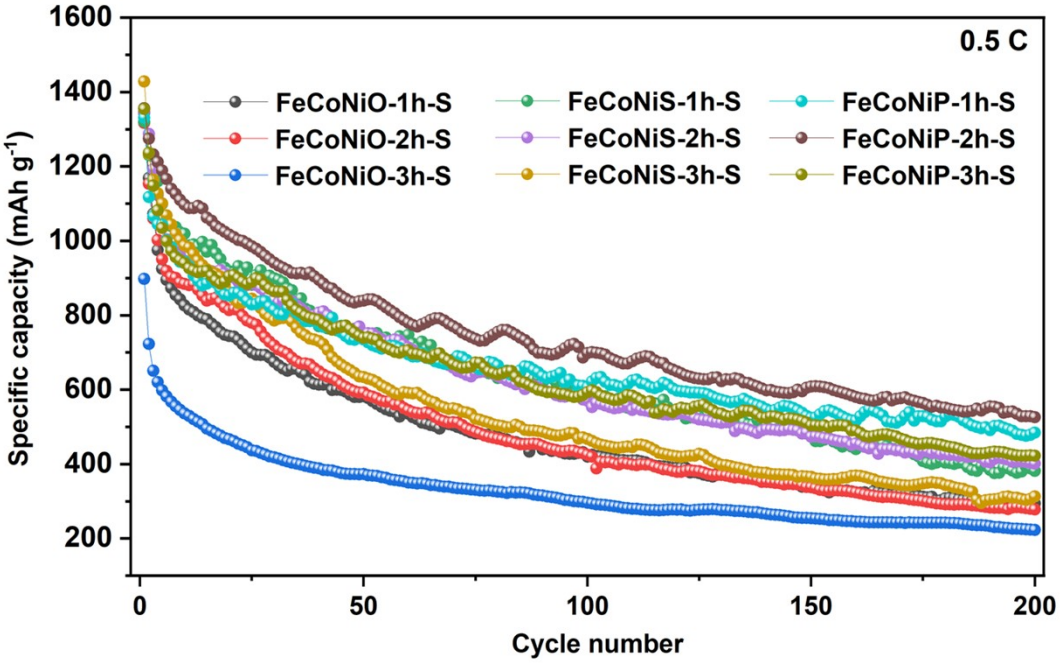

Figure S26. Cycle performance of FeCoNiO, FeCoNiS, and FeCoNiP at different calcination time.

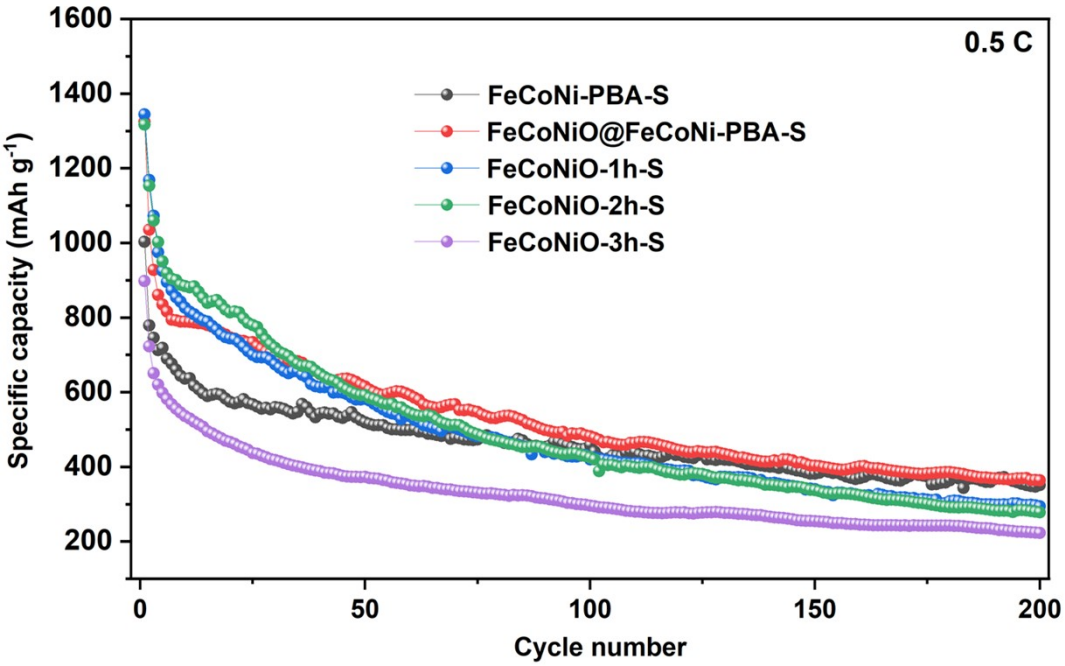

Figure S27. Comparison of cycle performance of FeCoNi-PBA-S, FeCoNiO-1h-S, FeCoNiO-2h-S, FeCoNiO-3h-S, FeCoNiO@FeCoNi-PBA-S.

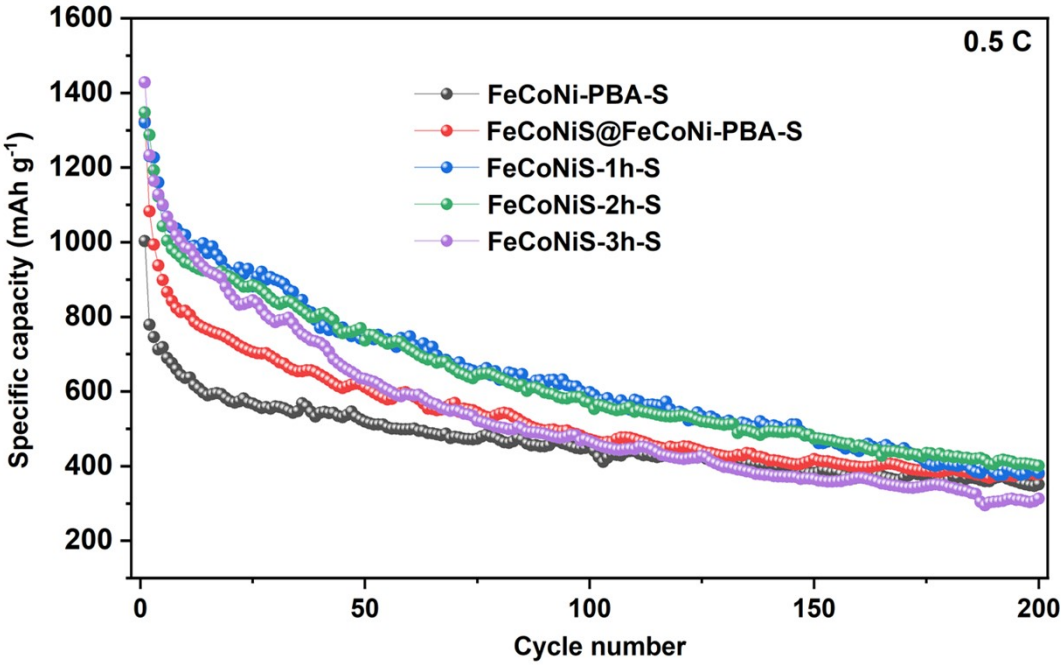

Figure S28. Comparison of cycle performance of FeCoNi-PBA-S, FeCoNiS-1h-S, FeCoNiS-2h-S, FeCoNiS-3h-S, FeCoNiS@FeCoNi-PBA-S.

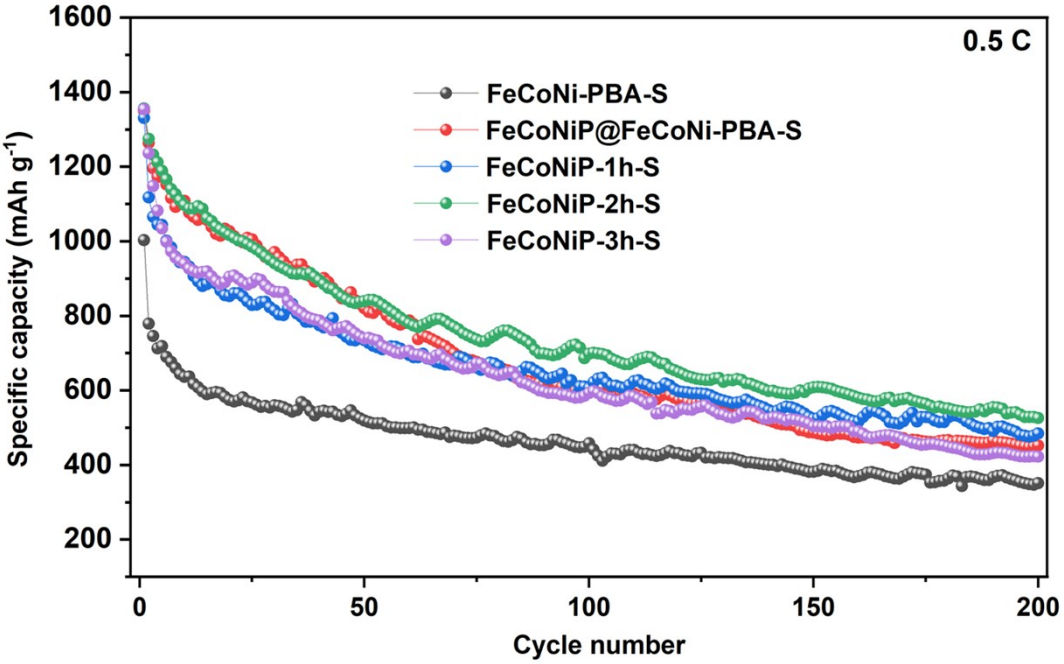

Figure S29. Comparison of cycle performance of FeCoNi-PBA-S, FeCoNiP-1h-S, FeCoNiP-2h-S, FeCoNiP-3h-S, FeCoNiP@FeCoNi-PBA-S.

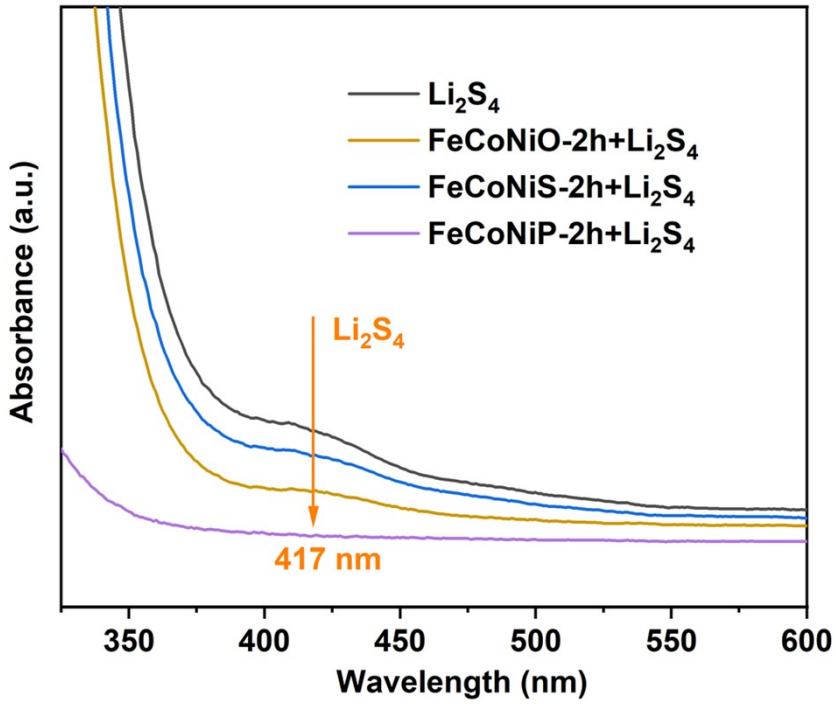

Figure S30. UV-vis spectra of Li_2S_4 solution before and after adsorption by FeCoNiO-2h, FeCoNiS-2h, and FeCoNiP-2h.

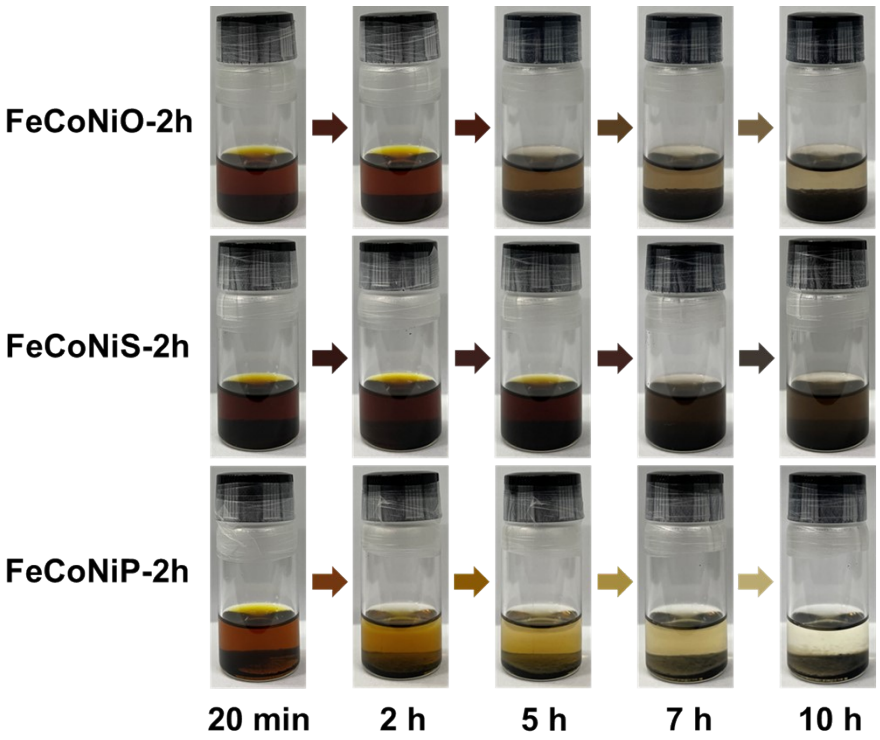

Figure S31. Optical photographs of Li_2S_4 solution permeation tests of FeCoNiO-2h, FeCoNiS-2h, and FeCoNiP-2h.

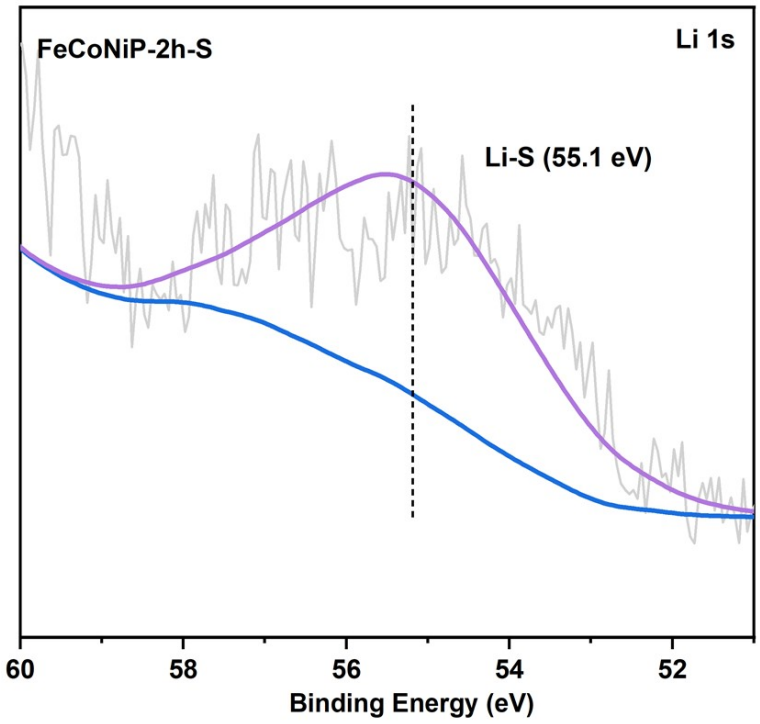

Figure S32. Li 1 s XPS spectra of FeCoNiP-2h powers after Li_2S_4 adsorption tests.

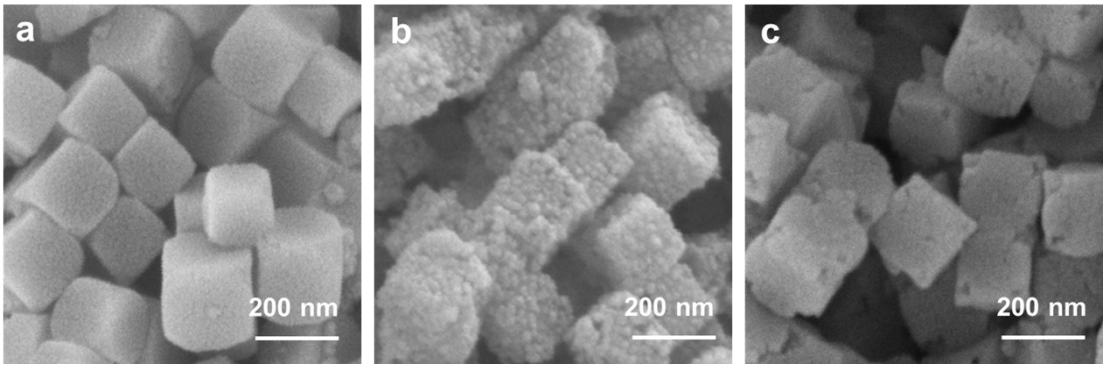

Figure S33. SEM images of (a) FeCoNiO-2h, (b) FeCoNiS-2h, and (c) FeCoNiP-2h after soaking in Li_2S_4 solution.

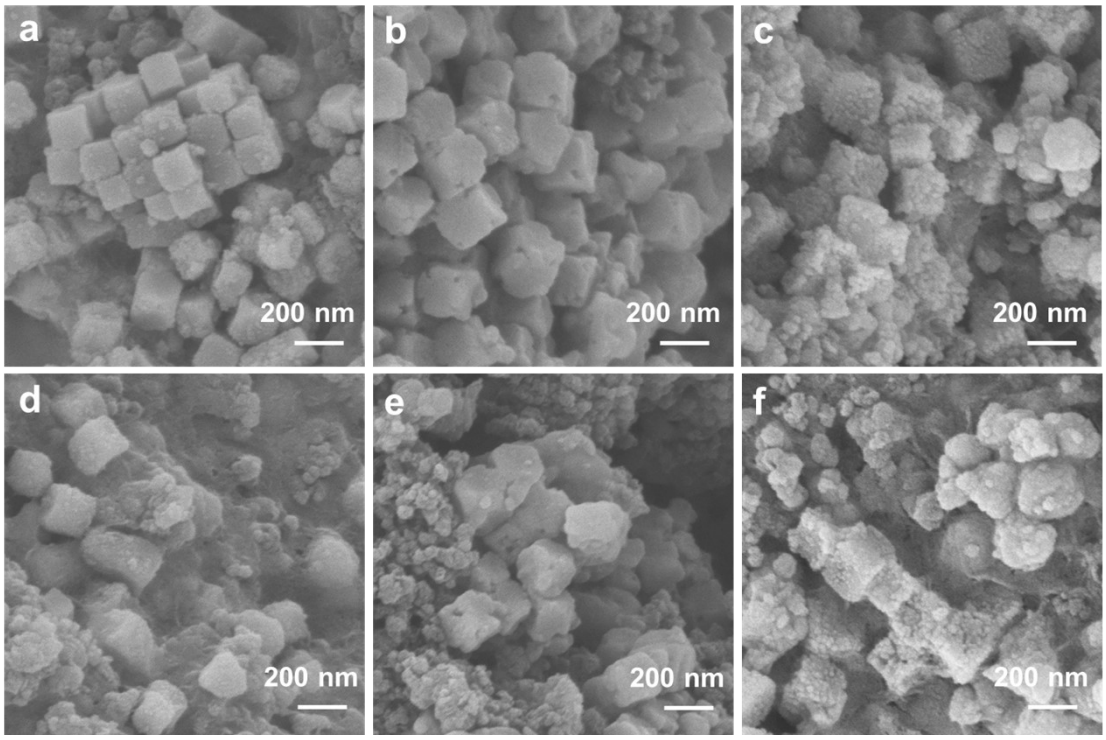

Figure S34. SEM images before cycling of (a) FeCoNiO-2h-S, (b) FeCoNiS-2h-S, and (c) FeCoNiP-2h-S. SEM images after 200 cycles at 0.5 C of (d) FeCoNiO-2h-S, (e) FeCoNiS-2h-S, and (f) FeCoNiP-2h-S.

Table S1. Elemental analysis data (mass fraction) of FeCoNi PBA-S, FeCoNiX-1h-S, FeCoNiX-2h-S, FeCoNiX-3h-S, FeCoNiO@FeCoNi-PBA-S, FeCoNiS@FeCoNi-PBA-S, and FeCoNiP@FeCoNi-PBA-S.

Samples	N (%)	C (%)	H (%)	S (%)
FeCoNi-PBA-S	1.36	7.87	8.64	70.26
FeCoNiO@FeCoNi-PBA-S	0.66	0.64	0.33	71.45
FeCoNiO-1h-S	0.63	0.58	0.53	70.58
FeCoNiO-2h-S	0.62	0.60	0.55	69.39
FeCoNiO-3h-S	0.54	0.66	0.48	69.35
FeCoNiS@FeCoNi-PBA-S	0.72	0.83	0.67	72.21
FeCoNiS-1h-S	0.53	0.51	0.53	74.04
FeCoNiS-2h-S	0.67	0.62	0.54	73.11
FeCoNiS-3h-S	0.54	0.59	0.33	74.34
FeCoNiP@FeCoNi-PBA-S	0.75	0.92	0.62	69.34
FeCoNiP-1h-S	0.61	0.63	0.32	70.34
FeCoNiP-2h-S	0.65	0.71	0.63	70.81
FeCoNiP-3h-S	0.55	0.65	0.49	69.91

Table S2. Comparison of the performances of reported metallic compounds as sulfur hosts for Li-S batteries.

Host Materials	Initial Capacity (mAh g^{-1})	Final Capacity (mAh g^{-1})	Cycles Number	Discharge Rate (C)	References
ACNF/Co_3S_4/S	957	550	100	0.3	[5]
$Zn_{0.30}Co_{0.31}Cu_{0.19}In_{0.13}Ga_{0.06}S$	706	480	100	0.2	[6]
S/C-HS@NiS	851	510	200	0.2	[7]
CoSP	700	568	100	0.2	[8]
FeP/rGO/CNTs-S	~650	~420	200	1	[9]
S@CoFeP@CN	~710	~450	200	0.5	[10]
CF/FeP@C@S	695	500	200	1	[11]
Al_2O_3/NiNCs-S	1556	496	200	0.5	[12]
S/$La_{0.8}Sr_{0.2}MnO_3$	792	532	150	0.1	[13]
NiMgCuZnCoO	890	479	600	0.5	[14]
FeCoNiP-2h-S	**1356.2**	**525.8**	**200**	**0.5**	**This**

References

1 G. Kresse and D. Joubert, *Phys. Rev. B*, 1999, **59**, 1758–1775.

2 G. Kresse and J. Furthmüller, *Phys. Rev. B*, 1996, **54**, 11169–11186.

3 J. P. Perdew, K. Burke and M. Ernzerhof, *Phys. Rev. Lett.*, 1996, **77**, 3865–3868.

4 S. Grimme, J. Antony, S. Ehrlich and H. Krieg, *J. Chem. Phys.*, 2010, **132**, 154104.

5 H. Xu and A. Manthiram, *Nano Energy*, 2017, **33**, 124–129.

6 M. J. Theibault, C. R. McCormick, S. Lang, R. E. Schaak and H. D. Abruña, *ACS Nano*, 2023, **17**, 18402–18410.

7 C. Ye, L. Zhang, C. Guo, D. Li, A. Vasileff, H. Wang and S. Qiao, *Adv. Funct. Mater.*, 2017, **27**, 1702524.

8 X. Chen, X. Ding, H. Muheiyati, Z. Feng, L. Xu, W. Ge and Y. Qian, *Nano Res.*, 2019, **12**, 1115–1120.

9 S. Huang, Y. Von Lim, X. Zhang, Y. Wang, Y. Zheng, D. Kong, M. Ding, S. A. Yang and H. Y. Yang, *Nano Energy*, 2018, **51**, 340–348.

10 C. Zhang, R. Du, J. J. Biendicho, M. Yi, K. Xiao, D. Yang, T. Zhang, X. Wang, J. Arbiol, J. Llorca, Y. Zhou, J. R. Morante and A. Cabot, *Adv. Energy Mater.*, 2021, **11**, 2100432.

11 J. Shen, X. Xu, J. Liu, Z. Liu, F. Li, R. Hu, J. Liu, X. Hou, Y. Feng, Y. Yu and M. Zhu, *ACS Nano*, 2019, **13**, 8986–8996.

12 P. Geng, Y. Lin, M. Du, C. Wu, T. Luo, Y. Peng, L. Wang, X. Jiang, S. Wang, X. Zhang, L. Ni, S. Chen, M. Shakouri and H. Pang, *Adv. Sci.*, 2023, **10**, 2302215.

13 Y. Liu, S. Liu, G. Li, T. Yan and X. Gao, *Adv. Sci.*, 2020, **7**, 1903693.

14 Y. Zheng, Y. Yi, M. Fan, H. Liu, X. Li, R. Zhang, M. Li and Z.-A. Qiao, *Energy Storage Mater.*, 2019, **23**, 678–683.